Fizika Nizkikh Temperatur, 2010, v. 36, No. 5, p. 532–548

Phonons of solid phases (α, β, δ, ε) of carbon monoxide by optical studies

A. Serdyukov[1,2], M. Vetter[1], A. Brodyanski[1,3], and H.J. Jodl[1]

[1] *Fachbereich Physik, TU Kaiserslautern, Germany*

[2] *Physikalisch-Technische Bundesanstalt, Abbestrasse 2–12 D-10587 Berlin-Charlottenburg, Germany*

[3] *Institut fuer Oberflaechen- und Schichtanalytik (IFOS) an der TU Kaiserslautern, Germany*
E-mail: anton.serdyukov@ptb.de

Received October 26, 2009

The phase diagram of solid carbon monoxide was investigated in the pressure range 0–10 GPa and temperature range 30–300 K by infrared and Raman spectroscopy. The tentative phase diagram known from literature was expanded and specified in details. The δ-phase region is divided into two subphases — δ_{rot} and δ_{loc} that is similar to the one in solid nitrogen. The pressure-temperature behavior of the elementary and combined excitations was also followed up. The vibron overtone region was carefully investigated by FTIR spectroscopy as a function of temperature at different pressures, whereas the fundamental one — by Raman spectroscopy. The features of the IR-active phonon sideband to the vibron overtone were investigated in details in the whole pressure-temperature region. The lattice-phonon spectra were studied by Raman spectroscopy as a function of pressure (at lowest temperature) and by IR spectroscopy as a function of temperature at saturated vapor pressure.

PACS: 33.20.Ea Infrared spectra;
33.20.Fb Raman and Rayleigh spectra (including optical scattering);
33.20.Vq Vibration-rotation analysis.

Keywords: Carbon monoxide, lattice phonons, phonon sideband, phase diagram, infrared spectroscopy, Raman spectroscopy.

Introduction

In last decades a lot of interest was taken to investigate the simple molecular systems such as H_2, N_2, O_2, CO_2 [1–3] (optical spectroscopic and structural studies, lattice dynamics, molecular dynamics, *ab initio* calculations, etc.). As yet only a few papers were dedicated to the solid CO within the last 50 years. The reason for this situation is probably the technical and experimental difficulties, connected with the studies of carbon monoxide (see later). CO is very often compared with the N_2, due to similarities in their molecular properties (same mass, same number of electrons). But in contrast to N_2 phase diagram, which is well studied, CO phase diagram remains almost completely unknown. There is only one version of the phase diagram known from the literature [4] in which only a small part of phase boundaries is determined experimentally, the rest of them was only estimated, perhaps by analogy with the nitrogen phase diagram known at that time (see Fig. 1).

Most of the studies of carbon monoxide are performed at ambient pressure. Raman spectra of vibrons and phonons at low temperature are published in the paper of Anderson et al. [5], Raman spectra of phonons in pure CO and mixture N_2–CO — in the paper of Witters et al. [6]. Far-infrared spectra of phonons at $T = 10$ K in pure CO can be found in papers of Anderson et al. [7] and Ron et al. [8], and both in pure CO and CO–N_2 mixtures in Fugol et al. [9]. Mid IR spectra of fundamental vibron plus phonon sideband are presented in the paper of Ewing et al. [10], and of overtone vibron plus phonon sideband in Legay et al. [11] (at 20 K and saturated vapor pressure). Only two papers are published on experimental investigations of CO under pressure (< 10 GPa) and at different temperatures (< 300 K) — x-ray structural analysis by Mills at al. [4] and Raman studies by Katz et al. [12] (the only known vibron and phonon spectra of high pressure phases). There are also few theoretical investigations on solid CO. Zumofen [13] modeled the experimentally known vibron splitting (*A–T* in Raman, LO-TO splitting of *T* mode in IR), the phonon sideband to vibron and optical phonons by a phenomenological potential and solid-state physics approach.

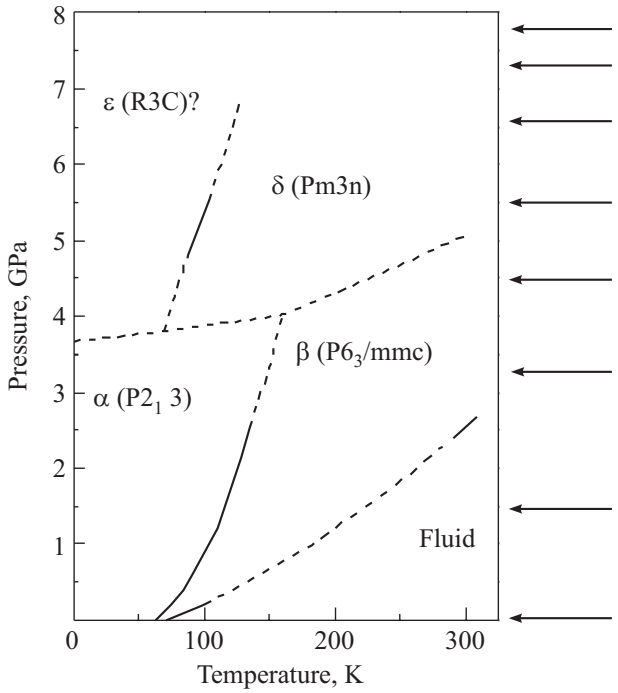

Fig. 1. *P–T* diagram for solid CO [4]: solid lines are phase boundary lines known from structural studies, dashed lines are estimated phase lines. Arrows on the right side indicate our isobaric investigations during cooling.

The different variants of lattice dynamics calcu-lations taking in account many specific aspects (such as *ab initio* potential, mass-asymmetry of molecule, translation-rotation coupling, lattice distortions, anharmonicity, etc.) were carried out by several authors [14–19] to model the experimentally known optical phonons and to suggest a phonon DOS (Fig. 2 summarizes these results).

As a resume of literature (Figs. 1, 2) one can draw that: (i) the phase diagram *P–T* should be investigated in details and the conclusions of [4,12] should be checked, (ii) a *P–T* behavior of elementary excitations (lattice phonons, vibrons) as well as phonon sideband should be followed up.

As it was mentioned above, there are some difficulties connected with the study of carbon monoxide. First, the gas is toxic, so the precautions should be taken during the loading of the cell. Second, the fundamental vibron absorption (~2140 cm^{-1}) is very strong and is saturated, unless the sample thickness is less than 10 μm. In addition, this absorption is falling into the broad diamond absorption of high-pressure cells (2100–2300 cm^{-1}). Solid CO at ambient pressure and low temperatures generates broad inhomogeneous bandwidth in optical spectra due to strong translation-rotation-coupling and head-tail disorder (CO, OC) (e.g. [7]). Furthermore, at pressures higher than 3 GPa and ambient temperature CO transforms irreversibly under the laser irradiation to dark red polymeric structure [4,12].

a

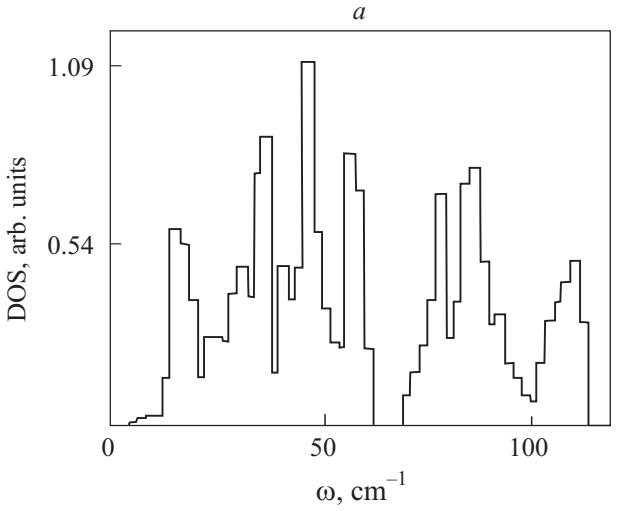

b

Mode frequency, cm^{-1}		Activity	Mode
Experiment	Theory		
38[2]	35.8[15]	Raman	LT
44[2]	43.4[13], 45.7[15]	Raman	LT
49, 50.5, 52[2,4,5]	46.4[13], 62[15]	Raman[4,5], IR[2]	T
58[2]	59.2[13], 56.4[15]	Raman	LT
64.5[2]	72.7[13], 74.4[15]	Raman	LT
85, 86[4,5]	84.9[13], 87.2[15]	IR	LT
90.5[2]	114.6[13], 98.3[15]	Raman	T

Fig. 2. Calculated phonon DOS for α-CO [16]: several maxima in the frequency regions of translational and librational phonons (see table) as well as the band edge at higher frequencies can be seen (*a*). Collection of lattice frequencies (in cm^{-1}) at **k** = 0 by Raman and far IR studies obtained by different authors in comparison to theoretical values (L — libration, T — translation, LT — mixed libration-translation). Experimental data are taken from references [5,7,8], calculated values (harmonic approximation, $P2_13$ structure) — from references [16] (model intermolecular potential) and [18] (*ab initio* CO-CO potential) (*b*).

Our aims are:

— to establish a phase diagram at $P < 10$ GPa and $T < 300$ K from changes in optical spectra like we achieved successfully for N_2–O_2 system [20] and N_2–CO system [21];

— to measure lattice modes as a function of pressure;

— to measure the IR-active phonon sideband to internal vibrational excitations in high-pressure phases of solid CO;

— to compare results achieved for CO with much better investigated solid N_2 (e.g. [22,23]) (due to similarities between both systems);

— to promote by our experimental results further theoretical investigations on solid CO.

2. Experimental

Spectra were recorded in the far and middle IR regions by the FTIR spectrometer (Bruker IFS120 HR). A tungsten lamp as the light source, a Si on CaF_2 beam splitter, and a liquid nitrogen cooled InSb detector (accessible range 1850 to 9000 cm^{-1}) were used in our measurements in the middle IR region. An Hg-vapor lamp as light source, 25 μm-Mylar beam splitter, and liquid-He-cooled Ge-bolometer as detector were used for measurements in the far-infrared spectral region (accessible frequency region 10–100 cm^{-1}). Spectral resolution was 0.1–3 cm^{-1} depending on the bandwidth of interest.

Raman signal was excited by the 488.0 nm or 514.5 nm lines of an Ar^+ laser (with 200–300 mW on the sample) and the spectra were recorded by a triple spectrometer in conjunction with a CCD camera (Jobin Yvon T64000). Spectral resolution was better than 3.5 cm^{-1} for libron excitation and better than 1.5 cm^{-1} for vibron modes.

For IR measurements at ambient pressure we used the cell, made of copper and brass equipped with sapphire windows (sample thickness 1.1 mm, ∅ 10 mm,), which was mounted onto a cold finger of a closed cycle He-cryostat (for details see [24]). The cell was placed at the focus of IR beam in the sample chamber of the spectrometer (focus diameter of about 1 mm). Sample temperature in the range of 10–80 K was measured by a calibrated silicon diode, which was attached directly to the sample cell; an absolute accuracy of temperature registration was of about 0.1 K.

For measurements at high pressures with the IR technique, we used a membrane diamond-anvil cell (DAC), linked to the IR spectrometer directly. For that reason the FTIR system was modified: 1) the IR focus diameter was reduced to ~100 μm by a beam condensing optics; 2) the membrane DAC was connected to the cold finger of a closed cycle He-cryostat, which was inserted into the sample chamber of spectrometer (for details see [25]). Sample temperatures between 30 and 300 K were measured by a calibrated silicon diode attached directly to the gasket of DAC. Local pressure inside the DAC was determined by the standard Ruby technique; in the range below 10 GPa we achieved accuracy better than ± 0.1 GPa.

For measurements at high pressures with the Raman technique we used a membrane DAC mounted on the cold finger of a closed cycle helium cryostat (T = 30–300 K).

CO-gas (Air Liquide) had a purity of 99.98% with CO_2-gas as main impurity.

Sample preparation and cooling rates during measurements at ambient pressure followed the routine elaborated by us for other cryocrystals (see e.g. [26]). Crystal quality was monitored by visual observation and by the continuum transmission of light (intensity of the central burst of the interferogram in FTIR measurements).

For high-pressure experiments the DAC was cryogenically loaded with pure CO. Initial pressure in the cell after loading procedure was ~1 GPa. We used several isobaric cooling cycles (see Fig. 1), always trying to be within the P–T region corresponding to a cryocrystal state, i.e. to be below the cryocrystal-polymer phase boundary to avoid the polymerization of CO during measurements (see later Fig. 12). The cooling rates were ≈ 1°/min in liquid state, ≈ 0.2°/min in high-temperature phases and low-temperature phases and ≈ 0.02°/min at the temperatures, where the phase transitions were expected. Both the IR and Raman spectra were collected at selected temperature-pressure points during the pauses in the cooling (sometimes also warming) of the sample. A recording of a spectrum lasted typically for ≈15 min for the FTIR spectra, 30–60 min for Raman spectra of vibron modes and 2–10 hours for Raman spectra of lattice modes (depending on the Raman signal intensity). The profile of the individual spectral bands were fitted by a Voigt function by using standard fitting routine (PeakFit v. 4.06 software) to determine the band position and the corresponding bandwidth. To find out the positions of the features of the sideband we fitted its experimental spectra by several individual peaks possessing a Voigt profile (for details see the corresponding parts in Ch. 3).

3. Experimental results

By some selected middle-IR spectra (from 8 isobaric runs and five different samples) we would like to demonstrate two aspects:

— the determination of the phase transitions from changes in optical spectra;

— the observation of phonon sidebands to the vibron modes being directly connected to the lattice-phonon DOS (density of states) and an analysis of its features.

Extensive knowledge of the N_2 system will help us to clarify some questions concerning the properties of CO. One should also keep in mind the differences between two molecules (symmetric/asymmetric, different distribution of the charges in the molecules, etc.), which lead to different spectral features and thereby to differences in phase diagrams (e.g. an existence of γ-phase in nitrogen).

In Figs. 3–8 (P = 0 GPa, 1.6 GPa and 4.6 GPa) we present the spectra of the ν_3 mode (asymmetric stretching vibration) of ppm CO_2 impurity in CO (Fig. 3, 5, 7) and (0–2) overtone mode of CO (Fig. 4, 6, 8) together with corresponding phonon sideband. In addition to spectra, the band positions and bandwidths are shown in these figures as a function of temperature. In some cases the splitting of spectral bands is disregarded by us (e.g. splitting of ν_3 mode of CO_2 at ambient pressure, see Fig. 3). In these cases the band is treated as a whole (bandwidth and band position of one integrated peak, fitted by a Voigt function, are shown). Let us to begin a detailed analysis.

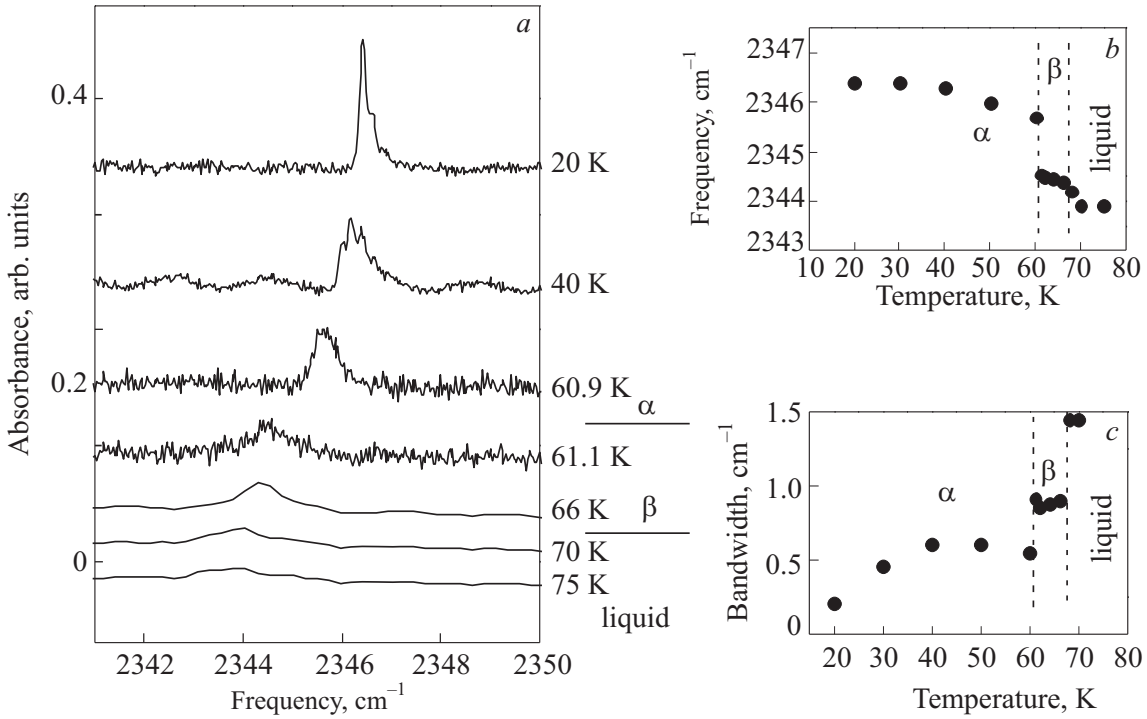

Fig. 3. Spectral results on matrix isolated CO_2 in CO at $P = 0$ GPa. IR spectra of ν_3-CO_2 mode collected during cooling as a function of temperature (*a*); evolution of frequency of the centre of mass of the band (*b*) and bandwidth (*c*) as a function of temperature. The splitting of the band is disregarded at this analysis and the band is treated as a whole. The numeric values of the experimental data points shown in Fig. (*b*) and (*c*) are presented in the Table 1 of the appendix A.

In Fig. 3,*a* we show IR spectra of the ν_3 mode of ppm CO_2 in CO during cooling at ambient pressure. Since we already used this probing technique with ppm CO_2 to study the α–β phase transition in N_2 successfully [27], we know all spectroscopic details of this mode such as band maximum, bandwidth, band intensity and splitting in solid N_2. Looking at the spectra (Fig. 3,*a*) in comparison to the ones in solid N_2 (Fig. 3 in α-N_2, Fig. 7 in β-N_2 of [27]) we observe one band in β-CO and one in α-CO at elevated temperatures. Nevertheless, in the low-temperature region of α-CO (lower 35 K) we observe an additional splitting of this mode probably due to the fact that the head-tail disorder of CO is frozen in (CO, OC molecules surrounding the probe molecule CO_2). However, these details will not be treated here and we only consider a behavior of the centre of mass of the whole band in our present analysis. The analysis of band position $\omega(T)$ and bandwidth $\Gamma(T)$ (Figs. 3,*b* and 3,*c*) as a function of temperature demonstrates a series of phase transitions: liquid (l) → β → α and confirms the temperatures of these phase transitions at $P = 0$ (see Fig. 1): $T_{l\beta}$ = (68.1±0.5) K and $T_{\beta\alpha}$ = (61.0±0.5) K (literature values: $T_{l\beta}$ = 68.1 K and $T_{\beta\alpha}$ = 61.6 K [1]).

In Fig. 4,*a* we present IR spectra of the (0–2) overtone region of CO (the absorption of the fundamental mode with the frequency $\nu_{0-1} \approx 2140$ cm^{-1} is too strong to be analyzed) during cooling at ambient pressure. Due to the big thickness of the sample in the «zero-pressure» cell (1.1 mm), the absorption of the (0–2) vibron mode is also saturated. At the β→α phase transition we recognize big changes in the bandwidth of this mode (which is estimated at the point of the maximum measured intensity, since the maximum of the intensity is cut due to saturation), a new band around 4280 cm^{-1} and a more structured phonon sideband. The physics of this new band was carefully studied by us [28] and the band is attributed to the absorption, caused by a coupling between two vibron modes, possessing different symmetry. This excitation (two-vibron band) exists due to symmetry considerations in α-CO only. From the plot in Fig. 4,*b* we determined the transition temperature β → α pretty accurately at 61.6 K. From Fig. 4,*a* it is not obvious how many features the sideband has at 60 or 50 K. To answer this question, we started our analysis with spectra taken at lowest temperature ($T \sim 11$ K), where the maxima in the sideband spectra are enough pronounced to be clearly identified, and applied this fitting pattern to the spectra at other temperatures. We found four maxima and the band edge at higher frequencies. The frequencies of these sideband features are presented in Fig. 4,*c* as a function of temperature.

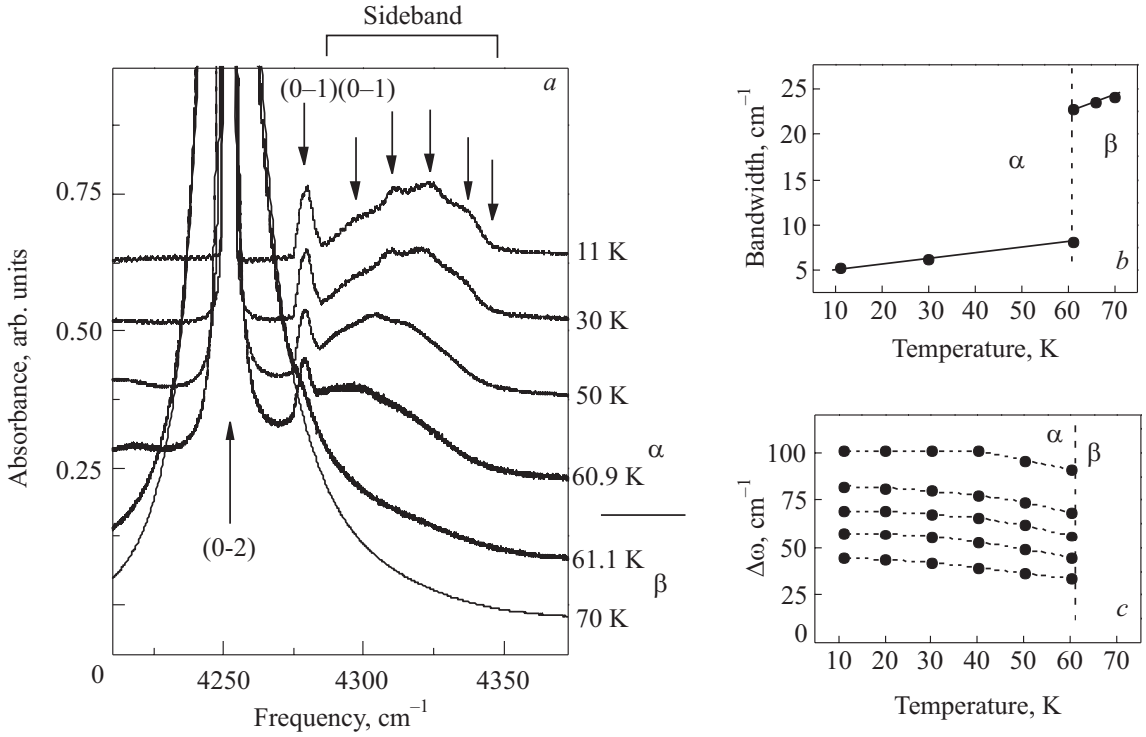

Fig. 4. Spectral results on CO overtone and overtone-sideband at P = 0 GPa. IR spectra in the overtone region of CO as a function of temperature: absorption band of the (0–2) mode of CO (saturated), of (0–1)(0–1) two-vibron mode of CO and phonon sideband to the overtone mode. (0–1)(0–1) mode, peaks in sideband and the band edge are depicted with arrows (*a*). Bandwidth of (0–2) mode of CO as a function of temperature. Since the IR peak of (0–2) band is saturated, the bandwidth was measured not at the half of the amplitude maximum but at the maximum of measured intensity (*b*). Evolution of frequencies of features and band edge in phonon sideband as a function of temperature; a Δω value is the difference between the frequencies of the respective feature in the sideband and the (0–2) vibron (*c*). Since the peaks in the sideband are not good resolved, the uncertainty in their position (frequency) is of about ±2 cm^{-1} at 20 K and rises by increasing the temperature (±5 cm^{-1} at 60 K). The position of the band edge is determined intuitively. The lines are serving as guides for eyes only. The values of the peak frequencies and bandwidths are presented in the Table 2 of the appendix A.

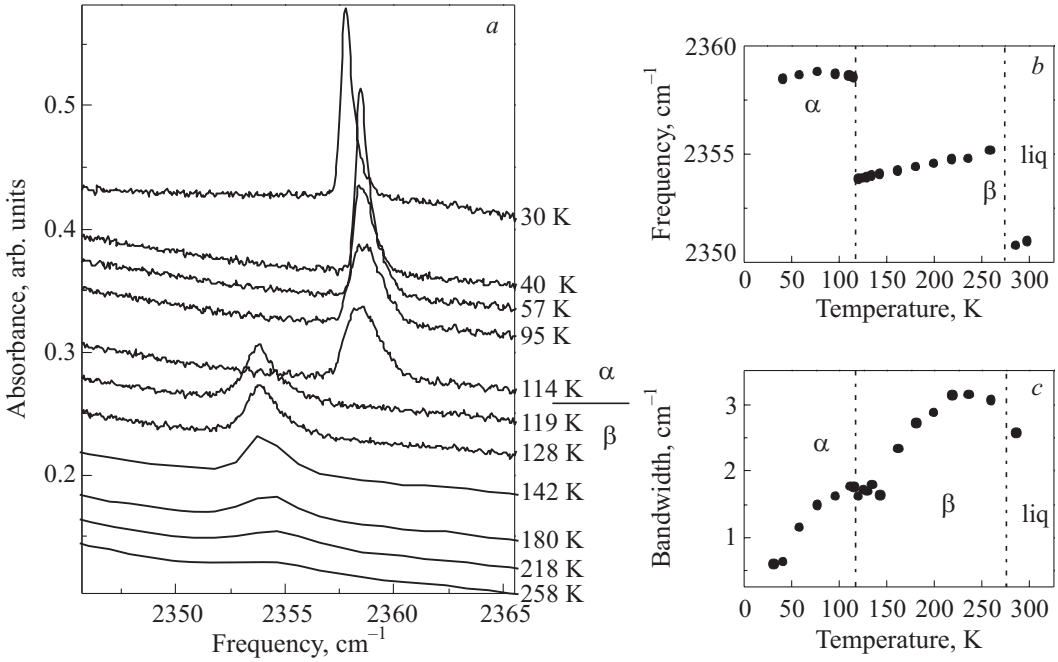

Fig. 5. Spectral results on matrix isolated CO_2 in CO at P = 1.6 GPa. IR spectra of ν_3-CO_2 in solid CO collected during cooling as a function of temperature (*a*); evolution of frequency of the centre of mass of the band (*b*) and bandwidth (*c*) as a function of temperature. The numeric values of the experimental data points shown in Fig. (*b*) and (*c*) are presented in the Table 3 of the appendix A.

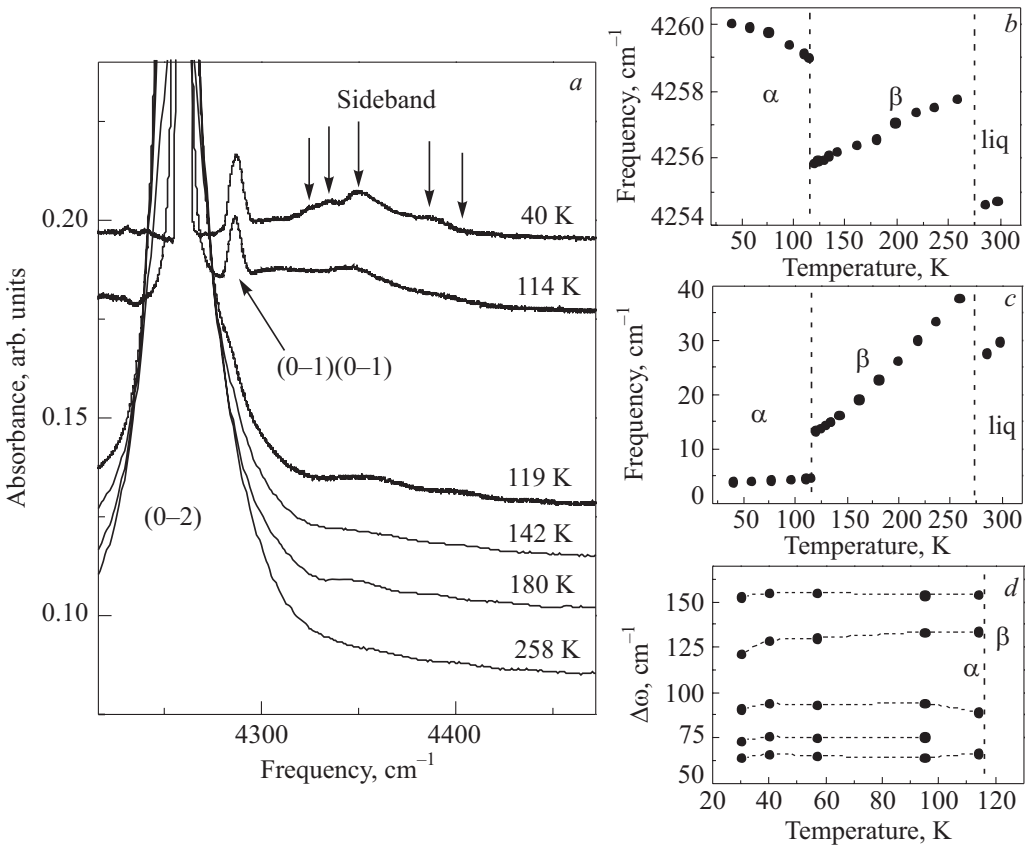

Fig. 6. Spectral results on CO overtone and sideband at P = 1.6 GPa. IR spectra in the overtone region of CO as a function of temperature: absorption band of the (0–2) mode of CO (saturated), of (0–1)(0–1) two-vibron mode of CO and phonon sideband to the overtone mode. (0–1)(0–1) mode, peaks in sideband and the band edge are depicted with arrows (*a*). Band position of (0–2) mode of CO as a function of temperature (*b*). Bandwidth of (0–2) mode of CO as a function of temperature. Since the IR peak of (0–2) band is saturated, the bandwidth was measured not at the half of the amplitude maximum but at the maximum of measured intensity (*c*). Evolution of frequencies of maxima and band edge of the phonon sideband ω(T) as a function of temperature; a Δω value is the difference between the frequencies of the respective feature in the sideband and the (0–2) vibron. Since the peaks in the sideband are not good resolved, the uncertainty in their position (frequency) is of about ±4 cm^{-1} at 30 K and rises by increasing the temperature (*d*). The position of the band edge is determined intuitively. The lines are serving as guides for eyes only. The values of the peak frequencies and bandwidths are presented in the Table 4 of the appendix A.

The results at 1.6 GPa are presented in Figs. 5 and 6 and analyzed in the same manner as those of Figs. 3, 4. As a result we find $T_{l\beta}$ (P = 1.6 GPa) at 270 K and $T_{\beta\alpha}$ (P = 1.6 GPa) at 115 K (see Fig. 12). As a phase transition temperature, we considered such temperature point wherein we could first clearly recognize sudden changes in spectra during cooling. How much the value found by us would differentiate from the actual phase transition temperature depends obviously on the temperature steps in the spectrum collection (5–10 K in our case) and on the degree of possible overcooling of the high-temperature phase at the cooling rate used. In comparison with literature: $T_{l\beta}$ ~ 270 K ($T_{l\beta}$ ~ ~ 230 K [4]) and $T_{\beta\alpha}$ ~ 114–116 K ($T_{\beta\alpha}$ ~ 116–118 K [4]).

Using the CO phase diagram from Mills et al. [4] as preliminary information, we successfully studied the phase sequence $\beta \rightarrow \delta \rightarrow$ ε-CO at 4.6 GPa during cooling process. In Fig. 7 we present spectra of ν_3-mode of ppm CO_2 in CO and their analysis. As before, from changes in band position ω(T) and bandwidth Γ(T) we can clearly indentify $T_{\beta\delta}$ ~ 170–180 K ($T_{\beta\delta}$ ~ 275 K [4]) and $T_{\delta\varepsilon}$ ~ 105 K ($T_{\delta\varepsilon}$ ~ ~ 80 K [4]). In Fig. 8 we show spectra (8,*a*) of the (0–2) CO overtone region and their analysis (8,*b*). In the spectra at low temperatures (T < 80 K) one can see one peak at ~ 4260 cm^{-1}, which has «shoulders» at both low and high frequency sides, three well resolved peaks between 4275 and 4305 cm^{-1} and some minor features. In the temperature region between 85 and 95 K the spectrum changes drastically — the shoulders of the band at 4260 cm^{-1} disappear as well as the three peaks at higher frequency become very broad and are strong overlapped. At this temperature point we claim the phase transition ε-δ.

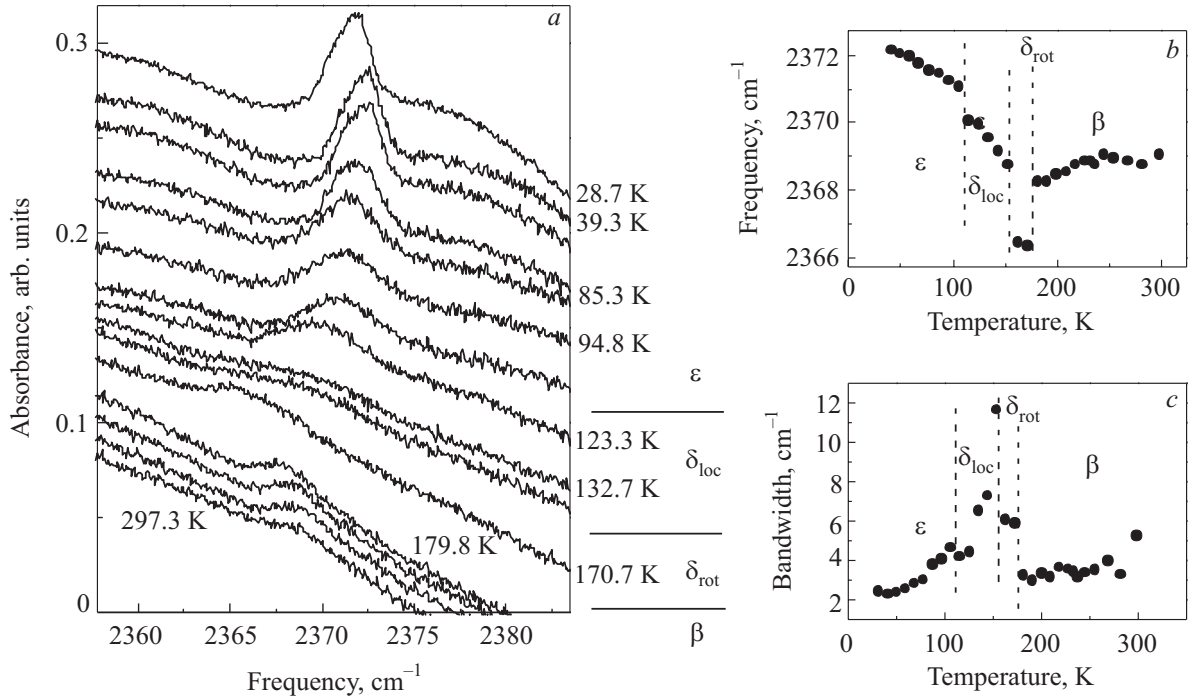

Fig. 7. Spectral results on matrix isolated CO_2 in CO at P = 4.6 GPa. IR spectra of ν_3-CO_2 band in solid CO collected during cooling as a function of temperature (*a*); evolution of frequency of the centre of mass of the band (*b*) and bandwidth (*c*) as a function of temperature. The numeric values of the experimental data points shown in Fig. (*b*) and (*c*) are presented in the Table 5 of the appendix A.

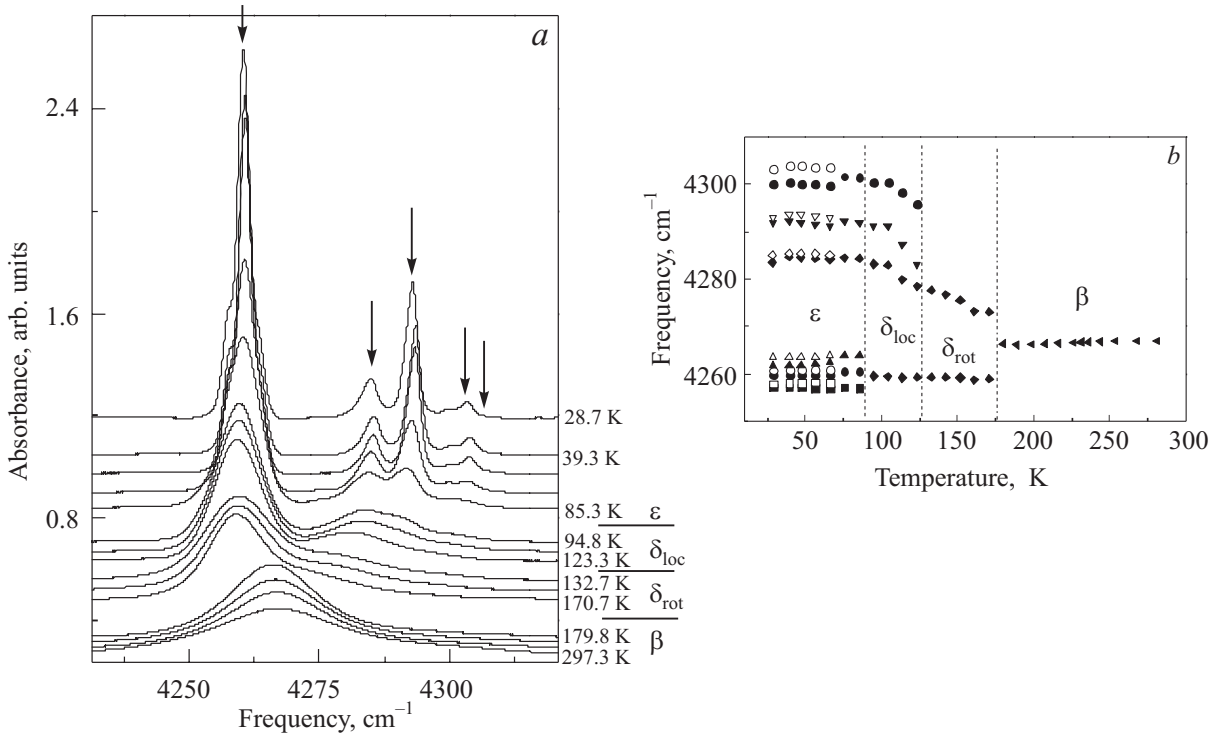

Fig. 8. Spectral results on CO overtone region at P = 4.6 GPa. IR spectra in the overtone region of CO as a function of temperature. Centre of the overtone band at ≈ 4260 cm^{-1}, and the bands at higher frequencies are depicted with arrows (*a*). Positions of the bands in the overtone region of the CO vibron mode as functions of temperature. Phase transition temperatures were determined from the visual changes in spectra and not from the frequency-temperature dependencies (*b*). The values of the peak frequencies and bandwidths are presented in the Table 6 of the appendix A.

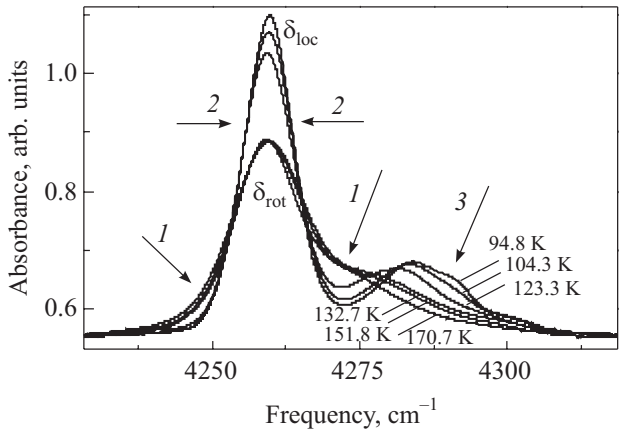

Fig. 9. Another representation of the spectra of (0–2) vibron plus phonon sideband of CO at 4.6 GPa in the temperature range 95–170 K (see Fig. 8,*a*) made to emphasize the changes in the spectra occurring during the phase transition between δ_{loc}- and δ_{rot}-phases. Arrows show the band profile regions, where these changes are most pronounced: bandshape (*1*); bandwidth (*2*); the high-frequency part (for details see text) (*3*).

Within the range of δ-phase (80–180 K at P = 4.6 GPa), we have the evidence of specific changes in the spectra at a certain temperature, indicating a possible phase transition. This situation is similar to solid N_2 where the δ-phase is divided into δ_{loc} and δ_{rot} phases (see next paragraph). In Fig. 9 we present IR spectra of the overtone range in the temperature interval of 95–170 K to stress minor but characteristic changes in the spectra occurring between 132.7 K and 123.3 K at cooling. It is: 1) the tail of the vibron mode peak at 4260 cm^{-1} becomes steeper — arrows *1* in Fig. 9; 2) this band narrows — arrows *2* in Fig. 9; 3) a high-frequency shoulder of this band transforms by jump first to one broad band (123.3 K), which is divided by following cooling into the three peaks in the spectral range of 4275–4305 cm^{-1}, — arrows *3* in Fig. 9.

The δ-phase of nitrogen, possessing eight molecules per unit cell, was studied carefully by Raman scattering and mid-IR absorption [22,29,30]. From changes in optical spectra, the δ-phase was divided into two parts: the high-temperature δ_{rot} phase, in which six N_2 molecules rotate as disks — so called disk-like molecules — and two ones rotate as spheres — sphere-like molecules, and the low-temperature δ_{loc}-phase, in which the disk-like N_2 molecules are frozen in whereas the sphere-like ones are not influenced. In carbon monoxide, we claim the similar situation: the δ-CO phase has two regions — the δ_{loc} phase (at lower temperatures) and the δ_{rot} phase (see Fig. 12,*a*).

One can see the results of the fitting (Peakfit) and the temperature evolution of the peaks measured at 4.6 GPa in Fig. 8,*b*. It would be obvious to assign the higher energy group of peaks (4275–4305 cm^{-1}) to the phonon sideband to the vibron overtone (0–2) if they were not so intensive

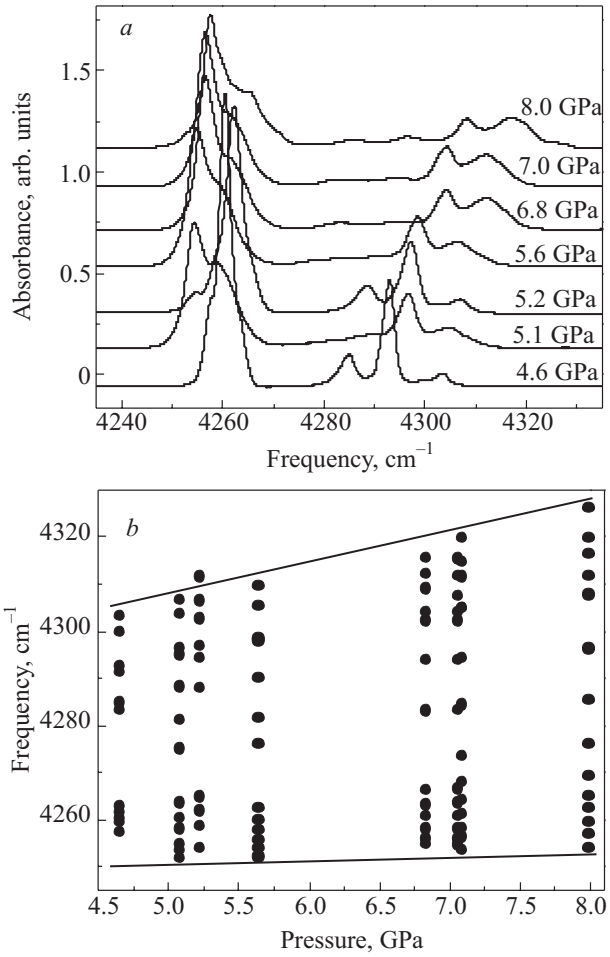

Fig. 10. IR spectra in the overtone region of CO in the ε-phase at low temperature (≈30 K) for some pressures (*a*) and analysis of the band positions as a function of pressure (*b*, see text). Thin lines are the guides for an eyes only.

in comparison to the vibron modes (a frequency region of 4260 cm^{-1}). For the fitting of the experimental spectra we assumed that there are 6 peaks at low temperature, and each of them is doubly splitted. It can be seen from the figure, that this splitting disappears at a certain temperature around 70 K. To clarify the origin of the high energetic group of peaks (4275 to 4305 cm^{-1}) we checked their pressure shift at low temperature in comparison to the low energetic ones (bearing in mind different frequency-pressure behavior of vibrons and phonons). The evolution of spectra with pressure is shown in Fig. 10,*a*, and the result of the above-mentioned analysis is shown in Fig. 10,*b*. It was not possible to follow every single peak at different pressures, but we could roughly determine the pressure shifts: 2–4 cm^{-1}/GPa for the first group (around 4260 cm^{-1}) and 4–7 cm^{-1}/GPa for the second group (4275–4305 cm^{-1}). The difference in pressure shift is not big, and there is no jump in frequency-pressure coefficient between bands at 4260 and 4270 cm^{-1}, therefore this analysis does not allow us to make the final conclusion. We will examine this issue

from another point of view later in the «discussion» section.

At this point we would like to review our experimental results. By measuring five different samples at various isobaric runs (P ~ 0, ~1.5, ~3, ~4.5 GPa) we completed investigation of the phase diagram in the selected P–T range in the mid IR spectral region. Our Raman spectra (Fig. 11,*a* vibron part, 11,*b* phonon part) confirm the scarce literature data at elevated pressure [12] and extend these results. There is an additional vibron splitting in δ- and ε-phases, except the expected sphere-disk splitting. Raman spectra of CO-lattice phonons at ambient pressure and low temperature show very broad bands due to all kinds of disorder [5,6]. At higher pressure these phonon bands are better resolved (Fig. 11,*b*). In β-phase there is one broad band due to orientational disorder. In α-phase we observed three modes i.e. the *E*, *T*, *T* phonons predicted in [13] (at 1.5 GPa in our spectra they are not very well resolved, the approximate positions are marked with arrows in Fig. 11,*b*). In ε-N_2 group theory predicted eight phonons ([23]); in ε-CO we recognize in Raman spectra at least four broad bands — which could be easily eight bands with a band width of about 10 cm^{-1} being typically for lattice modes. That much phonon modes (4) was also observed by Katz et al [12]. In opposite to the δ-N_2, where the Raman-active band caused by lattice phonons is clearly visible over a wide temperature range (Fig. 6 in [22]), the similar band in the δ-CO is not observable at all.

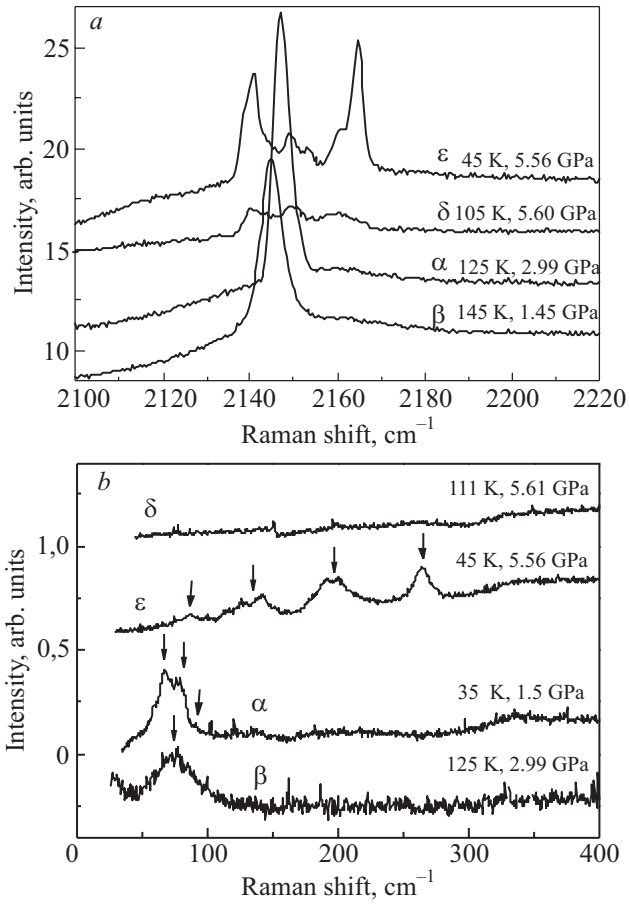

Fig. 11. Raman spectra of solid CO phases at different P–T values: fundamental vibron mode in different phases (*a*); phonon modes in different phases (phonon peaks are depicted with arrows, the broad feature in spectra at ≈ 350 cm^{-1} seems to be a fluorescent excitation of diamonds and disappeared from the spectrum when another laser wavelength was used) (*b*).

4. Discussion

4.1. P–T-phase diagram

On the basis of many data points (P_i, T_i) and the special technique — derivation of phase transitions from changes in optical spectra (see, e.g., [21]) — we were able to extend the tentative diagram by Mills [4] to a detailed one (Fig. 12,*a*). During cooling/warming cycles we were able to hold the pressure in the range ± 0.3 GPa (uncertainty in the pressure determination was about 0.2 GPa). The uncertainty in the determination of the phase transition temperature depends on the hysteresis of the phase transition temperature by cooling/warming, on the temperature steps between subsequent measurements before/after phase transition and on the accuracy of the temperature determination. Our observations showed that at low pressures the value of hysteresis amounts to the fractions of Kelvin, but at high pressure and low temperature can reach up to 10 K. In our «zero pressure» experiments we performed the measurements with very small temperature steps around the phase transitions (~0.2 K), and in the high pressure measurements the steps were ~5–10 K. The uncertainty of the temperature determination itself, due to the fact that the temperature sensor was located not directly in the sample, was considerable and varied with the temperature (bigger difference between the measured and real values at low temperatures) and with the experimental techniques (bigger difference between the measured and real values during Raman measurements due to laser heating). We confirmed the general character of the CO-phase diagram found by Mills et al. [4] but most of the slopes (dP/dT) are steeper in our case. The former δ-phase is now structured in two parts (δ_{rot}, δ_{loc}), like in solid N_2; the transition between δ_{rot}, δ_{loc} is presumably a second order transition.

As was already mentioned, solid CO transforms irreversibly into P–CO at higher pressure [4,12,31]. From spectral findings we were able to determine the transition to P-CO, which defines a thermodynamical stability conditions ($P_{critical}$ as a function of T). Since several technical parameters influence this transition, such as P, T, laser irradiation (energy, power, duration) and a percentage of CO in a mixture (in N_2-CO mixtures), we can establish different stability lines (Fig. 12,*b*). Using Raman scattering technique (wavelength 488 and 514 nm, power 100–500 mW), the transition from low temperature phases to P–CO can be determined by visual observation. The transparent sample turns into dark red, and the Raman signal of the CO vib-

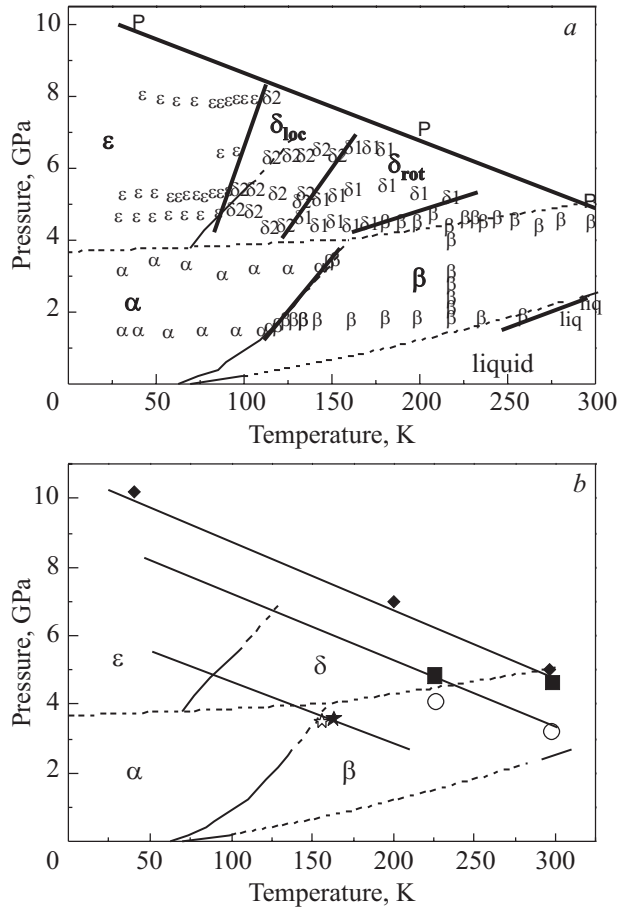

Fig. 12. Refined *P–T* diagram (thick lines are phase borders, determined in this work, thin lines are phase lines known from literature — see Fig. 1). Small Greek symbols represent our data points in each phase respectively. Thick line between α-, δ-, β-phases and «P» symbols represents the chemical stability line of CO molecule (*a*). CO phase diagram with the different lines of the thermodynamic stability of molecular crystal state (for details see text) (*b*). Each line is characteristic for the certain sample irradiation conditions: (i) by 488 nm laser (300–500 mW) in Raman scattering — opened star symbols before polymerization, closed star symbols after polymerization; (ii) by 514 nm laser (300–500 mW) in Raman scattering — opened circles and closed square symbols; (iii) by 630 nm laser (10 mW) in IR absorption studies — closed rhombuses. Some values at room temperature are known from literature [39,40] (which in general coincide with our values at room temperature, and therefore not shown).

ration disappears at a critical pressure. Using IR absorption technique, in combination with an additional laser diode (630 nm, 10 mW) to determine local pressure via Ruby fluorescence, one can observe the transition to *P*–CO by several spectral changes. First of all the CO mode (ν_{0-2}) decreases in intensity; additionally new modes (10–15) appear in spectrum and increase in intensity during the reaction. This topic is treated in details in another publication [32]. As a result we propose stability lines in Fig. 12,*b*, in which the laser-wavelength of irradiation of CO sample is varied. Our systematic studies confirm some existed values from literature [4]. The tendency is quite predictable — stability line moves to higher pressures and higher temperatures with smaller energy of irradiated photons. Remarkably, the position of the stability lines in the *P–T* diagram of CO lies at significantly lower temperature and pressure than in other simple molecular solids. For example in CO_2, transformation occurs at $P \sim 30$–80 GPa at $T \sim 2000$–3000 K [33], in N_2O at $P \sim 30$–60 GPa and 1500 K [34], and in N_2 at $P \sim 120$–200 GPa and 500–600 K [35].

Before we move on to the discussion of phonons and vibrons in different phases, we would like to clarify the origin of all bands in the vibron overtone region of the ε- and δ-phases of CO (we already started this discussion in the «experimental results» section). In Figs. 13 and 14 we present the comparative analysis of the phonon and vibron

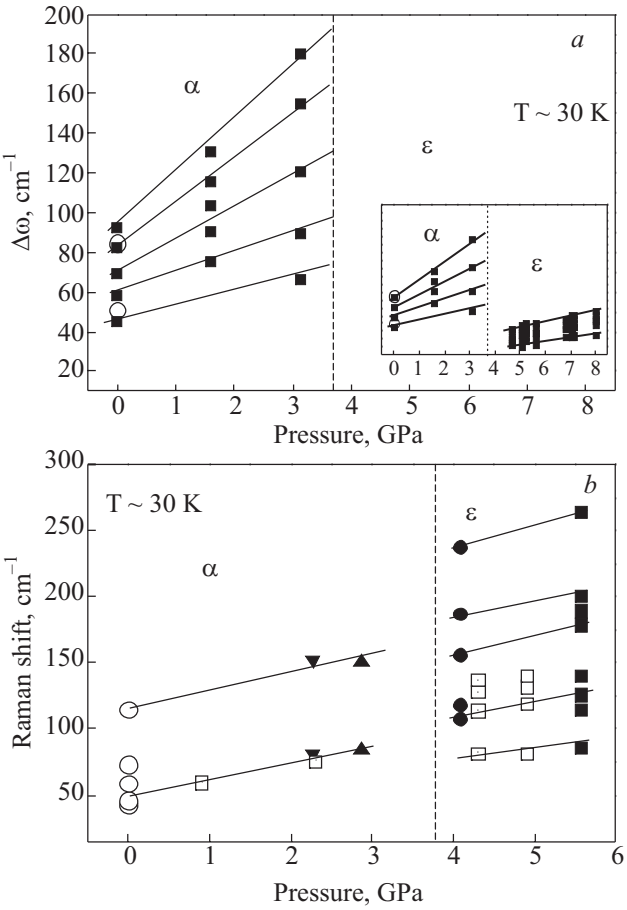

Fig. 13. Evolution of CO phonons (Raman, IR) and features in the phonon sideband (IR) with pressure: open circles – IR-active lattice phonons from [7,8] and closed squares — our data from IR phonon sideband, the inset shows the same dependencies for α-CO together with our data for ε-CO under an assumption that the peaks between 4280 and 4310 cm^{-1} in ε-phase are the features of the phonon sideband (for details see text) (*a*); Raman-active phonons (open circles from [6,7,13], open squares from [12] and closed symbols are our data from different samples) (*b*). Thin lines in both parts of the figure are guides for eyes only.

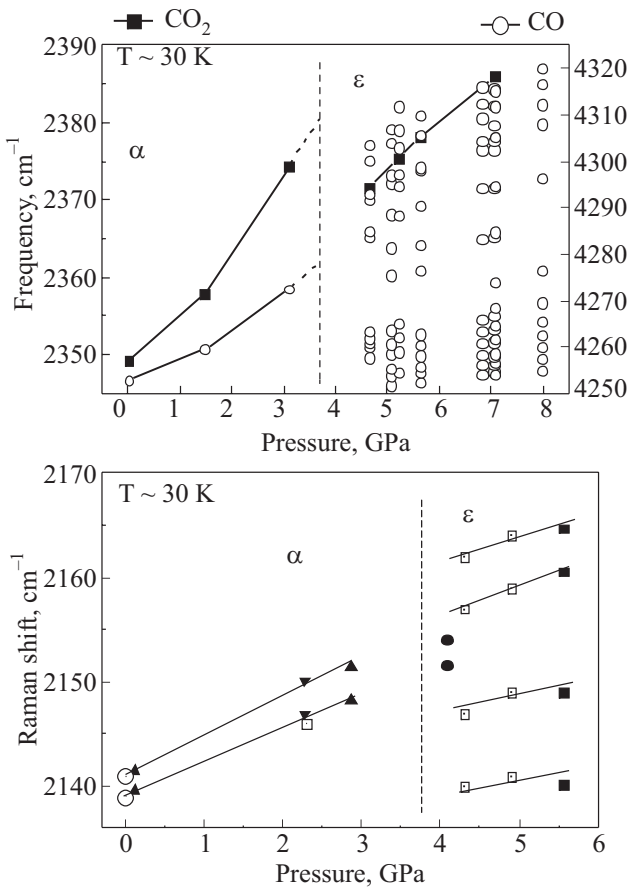

Fig. 14. Evolution of internal vibrational frequencies as a function of pressure: IR absorption data of CO overtone vibron mode (open circles, right scale) and ν_3 mode of CO_2 impurity molecules in solid CO (full squares, left scale). Values at $P = 0$ for CO are taken from [10] and for CO_2 from [39]. Dashed lines represent probable behavior of the vibron frequencies near the phase border (unknown due to lack of experimental points). Thin lines in ε-CO region are the guide for an eyes only (*a*). Raman vibron frequency-pressure dependencies. Values at $P = 0$ from [6] (open circles) and at $P > 0$ from [12] (open squares); full symbols mark our different samples. The values at $P = 4$ GPa are due to hysteresis and also due to a bit higher temperature (50 K) (*b*).

frequencies measured by Raman and infrared spectroscopy vs. pressure at low temperatures. Assuming that the peaks observed in ε-CO (Fig. 8,*a*) at the frequencies higher than 4280 cm^{-1} are actually features of the phonon sideband to the vibron group at of about 4260 cm^{-1}, we would get the negative frequency jump of 50–100 cm^{-1} (i.e. to smaller energies) at the phase transition α→ε (Fig. 13,*a* inset). However, the last conclusion would be inconsistent with the Raman results of the direct measurements of lattice phonon frequencies (Fig. 13,*b*), which show mainly splitting and no jump. Of course, the features in the phonon sideband (Fig. 13,*a*) should not coincide exactly with the simple sum of the frequencies of the vibron and phonon elementary excitations, but the frequency range of these features, being determined relative to the vibron mode, is usually roughly correspond to the frequency range of the phonons, measured by Raman spectroscopy.

To make sure of our assignment, we carried out an additional check: we reconstructed the vibron-overtone modes based on the fundamental ones measured directly by Raman spectroscopy (the overtone modes in Raman scattering are too weak to be observable in our measurements) and compared these to the experimental spectrum in the vibron-overtone spectral range measured by FTIR. Using the known experimental data for the α-CO at saturated vapor pressure (see, e.g., [28]) one obtains the simple relation between the vibron-overtone frequency (ω_{0-2}) und fundamental one (ω_{1-0}):

$$\omega_{0-2} \approx 2\omega_{1-0} - 25 \text{ cm}^{-1}.$$

Presupposing that this relation is approximately held in the ε-CO too we calculated the model vibron-overtone spectrum (Fig. 15, top) from the experimental Raman spectrum collected at 5.56 GPa and 45 K in the fundamental spectral region (Fig. 11,*a*, top). One can see (Fig. 15) that the model spectrum is very similar to the experimental spectrum taken by FTIR at 5.63 GPa and 31 K in this spectral region (previously already shown in Fig. 10,*a*). A decomposition of both spectra into single spectral bands (spectra shown by thin lines in Fig. 15)

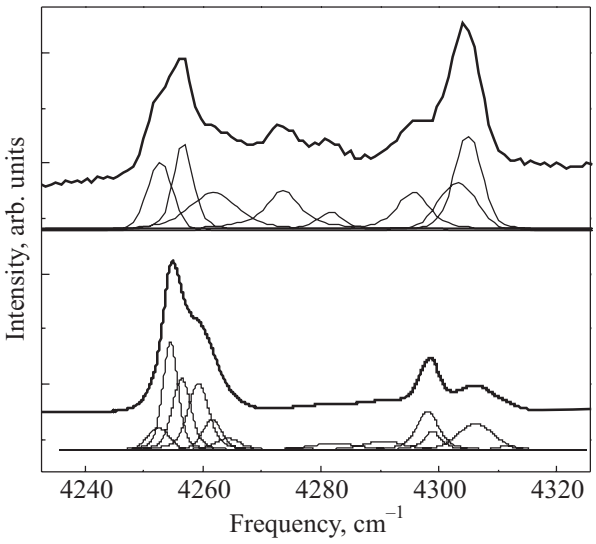

Fig. 15. Comparison of the IR spectrum of the (0–2) overtone region of CO in ε-phase at 5.63 GPa and 31 K (solid line, bottom) and of the reconstructed Raman vibron spectrum for this spectral region (solid line, top) based on the Raman spectrum of the fundamental region at 5.56 GPa and 45 K. Under each spectrum, the single bands obtained by decomposing the upper spectrum into individual ones are shown by thin lines. At fitting the Voigt function was used for every single band.

makes this similarity even more evident. The small differences between the modeled and experimental spectra in the intensity and the position of individual bands can be, to our opinion, traced to three main reasons. These reasons are: (i) inaccuracies in the experimental spectrum profiles (especially for the relatively weak Raman spectrum), (ii) various values of the resonance shift for different vibron modes and (iii) a different activity of the individual vibron modes in absorption (IR) and in Raman scattering. The last two circumstances can be important both for the fundamental and the vibron overtones.

Therefore, we assume that all peaks, observed by us in the FTIR spectrum in the ε and δ phases are vibrons. With this assumption, we get also the consistency between the Raman and infrared analysis of the vibron frequencies evolution at low temperatures (Fig. 14).

4.2. Phonons

Traditionally phonons are analyzed by inelastic neutron scattering throughout the whole Brillouin-zone or by optical spectroscopy at $\mathbf{k} = 0$ (elementary excitation absorption or scattering). From maxima in phonon sidebands and from the upper frequency of sideband in optical spectra (maximum energy of the phonon modes in the crystal) one gets some insight into the phonon DOS.

Using results of our FTIR studies, we were able to compare the phonon sideband to the fundamental mode of α-CO at saturated vapor pressure, measured by Dubost (quoted in [13]), with the one to the overtone (ν_{0-2}) of CO (see Fig. 4,*a* for $P \approx 0$ as well as Fig. 6,*a* at elevated pressure).

Figure 13 shows an evolution of phonon frequency ((*b*) — Raman data) and the frequency of the sideband features ((*a*) — FTIR) (which in fact are maxima of phonon DOS, modified by phonon-vibron interaction) with pressure at low temperatures for the α- and ε-CO phases.

To determine the position of sideband features and an upper band edge in IR spectra (Figs. 4,*c*; 6,*d*), we used the position of the (0–2) vibron overtone as a zero phonon line (ZPL, $\omega_{ph} = 0$) of the phonon sideband and defined $\Delta\omega(P)$ as a difference between the frequency of selected maximum and the ZPL. Values from literature are also integrated in Fig. 13 (see figure captions). From Raman spectra in the α-phase we observed an almost linear increase of phonon frequencies with pressure (10–15 cm^{-1}/GPa) of all three modes (*E*, *T*, *T*) (Fig. 13,*b*). From IR spectra in the α-phase we register a linear increase with pressure (10–30 cm^{-1} /GPa) of all 4 maxima in sideband and its band edge (Fig. 13,*a*). Between 3 and 4 GPa at 30 K we observe the α-ε phase transition. In the ε-phase we could not observe the phonon sideband in IR spectra, because it is partially covered by vibron peaks and most likely has too low intensity in comparison with the noise level and artefacts in spectra. The slope $\Delta\omega/\Delta P$ in ε-phase for the Raman modes is about 10–15 cm^{-1}/GPa similar to the one in the α-phase.

In general, these slopes $\Delta\omega/\Delta P$ within one phase can be related to the mode Grüneisen parameter γ. Unfortunately, we need the isothermal bulk modulus of CO for determination of γ, which is not known in α- and ε-CO.

4.3. Vibrons

From respective IR spectra we derived the vibron frequency as a function of pressure at $T \sim 30$ K for the (0–2) CO mode and for the ν_3 — CO_2 impurity mode in α- and ε-CO. In the same way we analyzed respective Raman spectra of several samples. The same analysis for the CO stretching mode was performed by Katz et al. [12]. For all vibron modes we observe a steep increase with pressure in α-CO, and a more flat increase with pressure in ε-CO (see Fig. 14,*a*,*b*). At the phase transition ($P \sim 3$–4 GPa) we observe a negative frequency jump for CO_2 vibron mode, and a multiple splitting for CO modes — at least four vibron modes in Raman spectra(Figs. 11 and 14,*b*) and more than ten modes in IR spectra (Figs. 8 and 14,*a*).

The Raman active mode in α-CO has an increase in frequency with pressure of $\Delta\omega/\Delta P \sim 3$ cm^{-1}/GPa. The slope of the IR active (0–2) overtone is 7–8 cm^{-1}/GPa, which means a $\Delta\omega/\Delta P \sim 4$ cm^{-1}/GPa for the fundamental mode (since we cannot measure the fundamental mode directly), i.e. both techniques gives practically the same values. The slope for the CO_2 impurity mode is about 10 cm^{-1}/GPa. For comparison, usually vibron modes possess a frequency shift with pressure at low temperatures of several cm^{-1}/GPa: in α-N_2 ~ 5 cm^{-1}/GPa, in ε-N_2 ~ ~ 2 cm^{-1}/GPa [23,36]. In the case of CO_2 the shift of its fundamental frequency with pressure is strongly influenced by the cage effect. I.e. since the impurity molecule is larger than the host molecule (the electronic cloud of the CO molecule has the dimension of 4×3 Å; CO_2 molecule 5×4 Å — Ref. 1), it causes a strong local deformation of its environment that increases by pressure and, thereby, a larger pressure shift arises. In the ε-CO both CO modes, i.e. (0–2) mode (IR data) and (0–1) mode (Raman data), possess a similar relative slope $\Delta\omega/(\omega\Delta P) \sim 2$–3 GPa^{-1}, and the ν_3-CO_2 impurity mode has a significantly larger (app. twofold) relative slope of ~ 6 GPa^{-1} similarly to the situation in the α-phase.

In Raman spectra (Fig. 11,*a*) we observe a splitting of vibron modes in ε-CO into at least 4 bands (top spectrum) being located in a narrow spectral region ($\Delta\omega \approx 20$ cm^{-1}) like in [12] at 15 K. The IR spectra of the low temperature ε-CO phase reveal a splitting into ~ 10 bands (see Figs. 8,*b*; 10). The spectra can be interpreted as six basic vibrons (3+3), each doubly split at low temperatures (below 70 K), or as the four basic vibrons (1+3), where the first mode at 4260 cm^{-1} is 6-fold split below 70 K and then 3-fold split up to the ε → δ phase transition. The splitting

at low temperatures can be caused by an appearance of a partial head/tail order of CO molecules in ε-CO.

By analogy with the δ-N_2 [22], the molecules, which are sphere-like in δ-CO (2 on site S_6) vibrate with frequency ν_1 (Raman active), the disk-like molecules (δ-CO, six on site C_2) vibrate with frequency ν_2 (2 × Raman active, 1 × IR active). In our experiments (Figs. 8, 11), we observed two IR-active modes ((0–2) mode splitting of 14–18 cm^{-1}) in the δ_{rot}-phase and 4 ones in the δ_{loc}-phase, where at least three Raman-active vibron modes are clearly recognizable. Since the details of the crystal structure and the site symmetry in the δ- and ε-phases of solid CO are not known, a concrete origin of the multitude vibron splitting observed by us in these CO-phases is not clear now.

4.4. Comparison between solid CO *and* N_2 *from optical studies*

We measured far IR spectra (20–100 cm^{-1}) of α-CO in the range 11–62 K and deduced band position ω(*T*) and band intensity especially for the T_u low-energetic mode (Fig. 16,*a*,*b*). Since the similar results are available for α-N_2 [37], we can perform a comparative analysis of the frequency behavior of the translational modes in both substances in the α-phase.

Because the signal to noise ratio in our spectra was relatively poor, we performed the standard smoothing procedure to remove the spikes on top of the bands due to high noise level. The results are presented in the Fig. 16,*a*. There are two peaks being clearly recognizable at low temperatures and showing systematic changes with temperature — at 50 cm^{-1} and at 86 cm^{-1} at 11 K. According to literature (see, e.g., [1]) we assigned these bands to $T_u^{(1)}$ and $T_u^{(2)}$ lattice phonon modes, respectively. The peak at ≈72 cm^{-1} shows no changes due to temperature (neither in its position nor in its shape nor in its intensity). Hence, we considered this peak as a measurements artefact caused, perhaps, by a modulation of the baseline of the liquid-He-cooled bolometer used. Due to the small peak absorbance of the $T_u^{(2)}$ mode, we analyzed the frequency behavior of the $T_u^{(1)}$ mode only. We extrapolated the temperature dependence of the frequency of this mode to 0 K and normalized the frequencies at other temperatures to this value (50.1 cm^{-1}). Then we applied the same analysis to the N_2 data from [37] and presented both dependencies on the same plot (Fig. 16,*b*). At 30 K (the highest temperature, at which the experimental data for N_2 are available) the relative changes in frequency are 3.4% and 2.2% for N_2 and for CO, respectively. In α-N_2 the main contribution to the phonon frequency shift with temperature is caused by increasing the molar volume [37]. A weaker thermal expansion of α-CO to compare to α-N_2 (p. 370 and 376 in [1]) can be an explanation of our results.

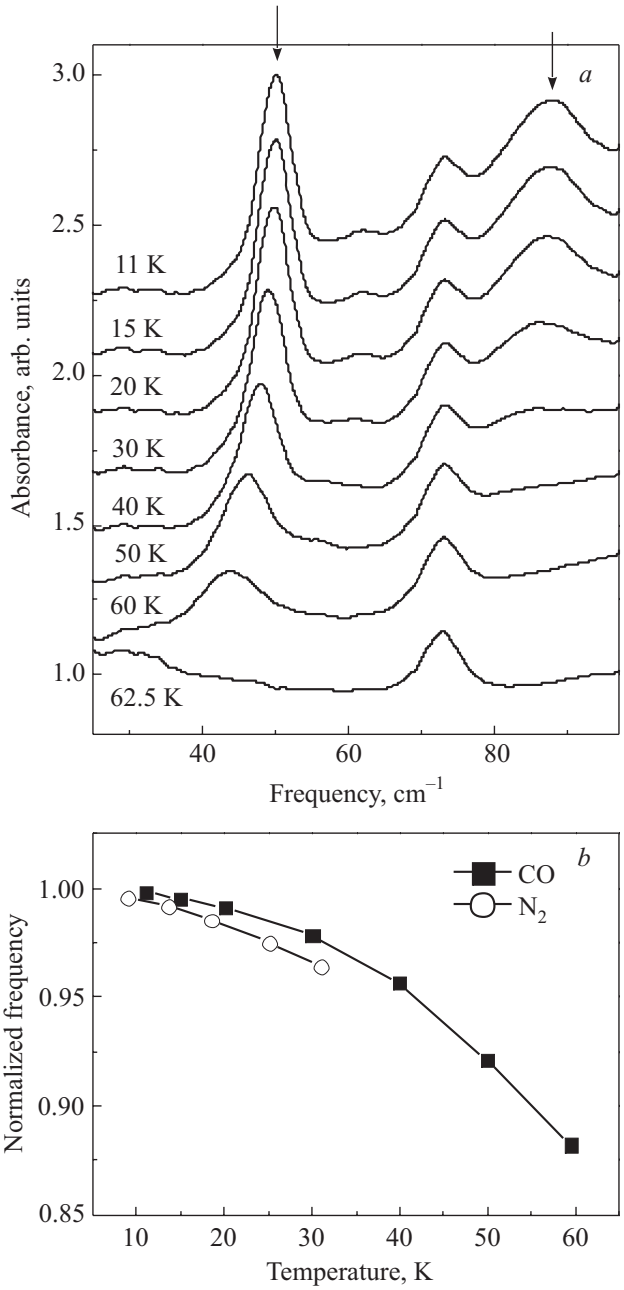

Fig. 16. Far IR spectra of α-CO as a function of temperature at saturated vapour pressure. Phonon peaks are depicted with arrows (*a*); normalized frequency ω(*T*)/ω(*T* = 0 K) of the low-energetic translational mode as a function of temperature (*b*)

We compared the phase diagram of solid N_2, known from structural and optical studies (Fig. 5 in [22]) with the diagram, refined by us, for solid CO from Fig. 12,*a*, and represent there together in Fig. 17. The slopes *dP*/*dT* of most phase boundary lines (liq/β, β/δ, δ/ε) are pretty similar. In solid N_2 there is the γ-phase between α- and ε-phase, but no counterpart in CO. Raich et al. [38] discussed this non-existence in details and claimed an existence of the γ-CO phase at higher pressure than in N_2. However, we

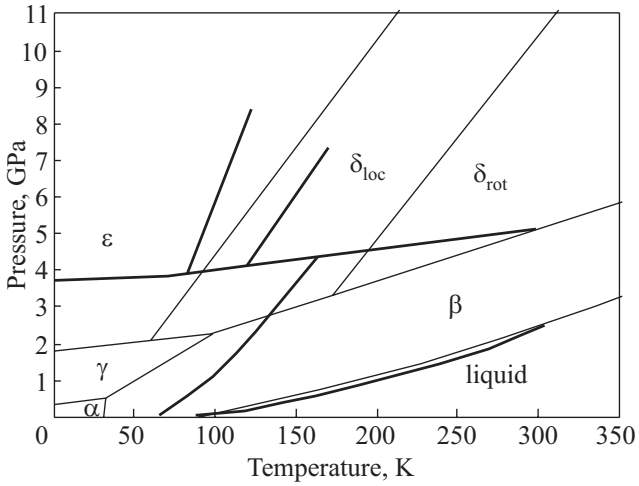

Fig. 17. Comparison of the *P–T* diagram of solid CO from our present optical studies (thick lines) to that of solid N_2 from literature [22] (thin lines). Greek symbols mark the phases of solid N_2 only. CO phase diagram is shown without the consideration of polymerization.

did not find this phase in CO within the whole region of the existence of the molecular CO (see Fig. 12,*b*). The region of δ_{loc} in solid CO is narrower than that for δ_{loc} in N_2. We speculate that the larger quadrupole moment (EQ) of CO to compare to N_2 can be a reason for it. The additional dipole–dipole (DD) interaction in CO is less relevant, because the energy of quadrupole–quadrupole interaction (EQ–EQ) is more than one order of magnitude larger than the energy of DD one [1].

5. Conclusion

The group of N_2-like molecular crystals was carefully studied by structural analysis, optical spectroscopy, thermodynamic investigations, but not solid CO. Hence, we studied almost ten samples of solid CO at pressures $P <$ < 10 GPa and low temperatures (10–300 K) by optical spectroscopy (mid- and far IR absorption, Raman scattering). We analyzed band position, bandwidth and integrated intensity of vibron and phonon modes of CO as well as impurity modes (ppm CO_2) as a function of pressure and temperature. To our knowledge, an analysis of the IR-active elementary excitation in the high-pressure phases of CO is carried out for the first time.

From several drastic changes in optical spectra we were able to identify phase transitions, including the irreversible transition to polymeric CO. We extended and precised the tentative *P–T*-phase diagram proposed in [4] based on the structural (x-ray) and Raman investigations. The CO-phase diagram established by us is principally similar to that of solid N_2 at elevated pressures with exception of the γ-phase, which does not exist in solid CO.

We confirmed an existence of at least four Raman-active vibron modes in ε-CO firstly reported in [12]. Three Raman-active vibron modes are established by us in the δ_{loc}-CO.

A plural splitting of the IR-active vibron mode is observed in the high-pressure phases of CO: two modes in δ_{rot}-CO, four modes in δ_{loc}-CO and up to twelve modes in ε-CO at low temperatures.

We relate this multitude of the vibron modes to either fine details of crystal structure of the high-pressure CO-phases (e.g., partial head-tail ordering of CO molecules and small distortion of the unit cell caused by it) or to the macroscopic electric effects such as LO–TO splitting, or to both effects together.

Concerning the lattice phonons at high-pressure we confirmed the only results of [12] for ε-CO.

We measured phonon frequencies in α-CO as a function of temperature at saturated vapour pressure. From the comparison with the similar data for α-N_2 we could draw both the similarity in this course for both substances and the quantitative difference in their temperature behavior that we connected to the differences in the thermal expansion of both crystals.

We acknowledge the financial support by the DFG (Grant number Jo 86–11).

Appendix A

The numeric results of the fit procedure.

Each table represents the numeric values of the data points shown in the corresponding Figure.

Table 1.

Figure 3, CO_2, 0 GPa

Temperature, K	Frequency, cm^{-1}	Linewidth, cm^{-1}
20	2346.4	0.21
30	2346.4	0.46
40	2346.3	0.61
50	2346	0.61
60	2345.7	0.55
61.1	2344.54	0.92
62	2344.49	0.86
64	2344.46	0.88
66	2344.38	0.91
68	2344.2	1.45
70	2343.9	1.45
75	2343.9	1.64

Table 2.

Figure 5, CO_2, 1.6 GPa

Temperature, K	Frequency, cm^{-1}	Linewidth, cm^{-1}
40	2358.5	0.62
57	2358.67	0.66
76	2358.85	1.17
95	2358.72	1.5
109.5	2358.64	1.64
114.3	2358.56	1.78
118.8	2353.87	1.77
123.5	2353.92	1.63
128.3	2353.95	1.73
133.3	2354.02	1.71
142	2354.1	1.81
161	2354.26	1.65
180	2354.42	2.35
198	2354.58	2.73
218	2354.79	2.89
235	2354.83	3.15
258	2355.17	3.17
285	2350.84	3.08
296.6	2351	2.59

Table 3.

Figure 7, CO_2, 4.6 GPa

Temperature, K	Frequency, cm^{-1}	Linewidth, cm^{-1}
39.3	2372.2	2.35
47.3	2372.1	2.45
56.5	2372	2.6
66	2371.8	2.89
75.5	2371.6	3.05
85.3	2371.5	3.84
94.8	2371.3	4.11
104.3	2371.1	4.72
113.8	2370.1	4.26
123.3	2370	4.48
132.7	2369.6	6.57
142.2	2369.2	7.34
151.8	2368.8	11.7
160.9	2366.5	6.14
170.7	2366.4	5.91
179.8	2368.3	3.28
188.9	2368.3	3
198.4	2368.5	3.4
207.5	2368.6	3.23
216.6	2368.8	3.71
226	2368.9	3.6
231.1	2368.9	3.5
235.6	2368.8	3.22
243.8	2369.1	3.42
253.3	2369	3.58
267.5	2368.9	4.02
280.5	2368.8	3.34
297.3	2369.1	5.31

Table 4.

Figure 4, CO overtone + sideband, 0 GPa

Temperature, K	Overtone Linewidth, cm^{-1}	Relative frequencies of the sideband features, cm^{-1}				
11	5.31	44.6	57.4	69.4	82.3	101
20		43.6	57	68.9	81.5	101
30	6.28	42.4	55.7	67.4	79.8	101
40		39.5	53.3	65.6	77.5	101
50		36.4	49.2	61.6	74.2	96
60	8.21	33.6	45.1	56.2	68	91
61.1	22.69					
62						
64						
66	23.5					
68						
70	24.14					
75						

Table 5.

Figure 6, CO overtone + sideband, 0 GPa

Temperature, K	Overtone frequencies, cm^{-1}	Overtone Linewidth, cm^{-1}	Relative frequencies of the sideband features, cm^{-1}				
296.6	4254.73	29.6898					
284.6	4254.63	27.5895					
258	4257.78	37.65982					
235	4257.54	33.41476					
218	4257.38	30.04525					
198	4257.07	26.13447					
180	4256.57	22.72514					
161	4256.39	19.12779					
142	4256.2	16.1495					
133.3	4256.05	15.00898					
133.3	4256.1	15.02389					
128.3	4255.95	14.34947					
123.5	4255.93	13.88943					
118.8	4255.87	13.33312					
114.3	4259.01	4.64279					
114.3	4259.0207	4.65234					
109.5	4259.13	4.53853	66.5	—	89.2	133.6	154
95	4259.4	4.37915	64	75.4	94.3	133.3	153.8
75.7	4259.78	4.20745	64.9	74.8	93.1	130.1	155.2
56.8	4259.93	4.09175	66.3	75.9	93.9	128.9	155.1
39.7	4260.06	3.96082	64	73.4	91	121.5	152.9

Table 6.

Figure 8, CO overtone , 4.6 GPa

Temperature, K	Vibron frequencies, cm^{-1}											
28.7	4257.28	4257.96	4259.81	4260.76	4261.83	4263.45	4283.59	4285.07	4291.87	4293.16	4300.09	4303.48
39.3	4257.3	4258.15	4259.97	4260.93	4261.89	4263.65	4284.74	4285.51	4292.25	4293.72	4300.44	4304.01
47.3	4257.28	4258.16	4259.98	4260.94	4261.89	4263.64	4284.62	4285.42	4292.04	4293.54	4300.31	4303.89
56.5	4257.04	4258.19	4259.89	4260.97	4262.09	4263.69	4284.39	4285.33	4291.73	4293.39	4300.02	4303.77
66	4256.84	4258.05	4259.75	4260.98	4262.32	4263.87	4284.26	4285.02	4291.35	4293.14	4299.83	4303.74
75.5	42577.22		4260.6		4263.87		4284.58		4292.21		4301.75	
85.3	4257.04		4260.54		4263.96		4284.31		4291.85		4301.49	
94.8			4259.55				4283.23		4291.31		4300.67	
104.3			4259.5				4282.92		4291.35		4300.59	
113.8			4259.16				4279.9		4287.3		4298.3	
123.3			4259.27				4278.49		4283.03		4295.84	
132.7			4259.34				4277.65					
142.2			4259.26				4276.75					
151.8			4259.21				4275.53					
160.9			4258.78				4273.22					
170.7			4258.91				4273.03					
179.8				4266.32								
188.9				4266.12								
198.4				4266.25								
207.5				4266.41								
216.6				4266.53								
226				4266.6								
231.1				4266.72								
235.6				4266.74								
243.8				4266.84								
253.3				4266.95								
267.5				4266.92								
280.5				4266.97								

1. V.G. Manzhelii and Yu.A. Freiman, *Physics of Cryocrystals*, AIP Press, Woodbury, New York (1996).
2. Russell J. Hemley, *Annu. Rev. Phys. Chem.* **51**, 763 (2000).
3. Yu. A. Freiman and H.J. Jodl, *Phys. Rep.* **401**, 1 (2004).
4. R.L. Mills , D. Shiferl, A.I. Katz, and B.W. Olinger, *J. Phys*. **11**/**45**, 187 (1984); R.L. Mills, B. Olinger, and O.T. Cromer, *J. Chem. Phys*. **84**, 2837 (1986).
5. A. Anderson, T.S. Sun, and M.C.A. Donkersloot, *Can. J. Phys*. **48**, 2265 (1970).
6. Kent R. Witters and J.E. Cahill, *J. Chem. Phys*. **67**, 2405 (1977).
7. A. Anderson and G.E. Leroi, *J. Chem. Phys*. **45**, 4359 (1966).
8. A. Ron and O. Schnepp, *J. Chem. Phys*. **46**, 3991 (1967).
9. I.Ya. Fugol', L.V. Khashchina, and I.M. Pritula, *Fiz. Nizk. Temp*. **13**, 185 (1987) [*Sov. J. Low Temp. Phys*. **13**, 102 (1987).
10. George E. Ewing and George C. Pimentel, *J. Chem. Phys*. **35**, 925 (1961).
11. F. Legay and N. Legay-Sommaire, *Chem. Phys*. **65**, 49 (1982).
12. llen I. Katz, David Shiferl and Robert L. Mills, *J. Phys. Chem*. **88**, 3176 (1984).
13. G. Zumofen, *J. Chem. Phys*. **68**, 3747 (1978).
14. Takako Shinoda and Hisae Enokido, *J. Phys. Soc. Jpn*. **26**, 1353 (1969).
15. Pier Francesco Fracassi and Michael L. Klein, *Chem. Phys. Lett*. **108**, 359 (1984).

16. Pier Francesco Fracassi, Roberto Righini, Raffaele Guido Della Valle, and Michael L. Klein, *Chem. Phys*. **96**, 361 (1985).
17. Pier Francesco Fracassi, Gianni Cardini, Séamus O-Shea, Roger W. Impey, and Michael L. Klein, *Phys. Rev.* **B33**, 3441 (1986).
18. W.B.J.M. Janssen, J. Michiels, and A. van der Avoird, *J. Chem. Phys*. **94**, 8402 (1991).
19. T.N. Antsygina, V.A. Slusarev, Yu. A. Freiman, and A.I. Erenburg, *J. Low Temp. Phys.* **56**, Nos. 3/4 (1984).
20. M. Minenko and H.-J. Jodl, *Fiz. Nizk. Temp*. **32**, 1382 (2006) [*Low Temp. Phys.* **32**, 1050 (2006)].
21. M. Vetter, A. Brodyanski, and H.-J. Jodl, *Fiz. Nizk. Temp*. **33**, 1383 (2007) [*Low Temp. Phys.* **33**, 1052 (2007)].
22. Roberto Bini, Mattias Jordan, Lorenzo Ulivi, and Hans J. Jodl, *J. Chem. Phys*. **108**, 6849 (1998).
23. R. Bini, L. Ulivi, J. Kreutz, and H.J. Jodl, *J. Chem. Phys*. **112**, 8522 (2000).
24. M. Minenko, M. Vetter, A.P. Brodyanski, and H.J. Jodl, *Fiz. Nizk. Temp*. **26**, 947 (2000) [*Low Temp. Phys.* **26**, 699 (2000)].
25. R. Bini, R. Ballerini, G. Pratesi, and H.J. Jodl, *Rev. Sci. Instrum*. **68 (8)**, 3154 (1997).
26. A.P. Brodyanski, S.A. Medvedev, M. Vetter, J. Kreutz, and H.J. Jodl, *Phys. Rev.* **B66**, 104301 (2002).
27. Martin Vetter, Matthias Jordan, Alexander P. Brodyanski, and Hans J. Jodl, *J. Phys. Chem*. **104**, 3698 (2000).
28. M. Vetter, A.P. Brodyanski, S.A. Medvedev, and H.J. Jodl *Phys. Rev.* **B75**, 014305 (2007).
29. M.I.M. Scheerboom and J.A. Schouten, *Phys. Rev. Lett*. **71**, 2252 (1993).
30. Leonardo Tassini, Federico Gorelli, and Lorenzo Ulivi, *J. Chem. Phys*. **122**, 74701 (2005).
31. W.J. Evans, M.J. Lipp, C.-S. Yoo, H. Cynn, J.L. Herberg, and R.S. Maxwell, *Chem. Matter* **18**, 2520 (2006).
32. Matteo Ceppatelli, Anton Serdyukov, Roberto Bini, and Hans J. Jodl, *J. Phys. Chem*. **B113**, 6652 (2009).
33. Mario Santoro, Jung-fu Lin, Ho-kwang Mao, and Russell J. Hemley, *J. Chem. Phys*. **121**, 2780 (2004).
34. V. Iota, J-H. Park, and C.S. Yoo, *Phys. Rev.* **B69**, 064106 (2004).
35. Eugene Gregoryanz, Alexander F. Goncharov, Russell J. Hemley, Ho-kwang Mao, Maddury Somayazulu, and Guoyin Shen, *Phys. Rev.* **B66**, 224108 (2002).
36. H.J. Jodl et al., *J. Chem. Phys*. **76**, 3352 (1982).
37. R. Bini, *J. Chem. Phys*. **104**, 4365 (1996).
38. J.C. Raich and R.L. Mills, *J. Chem. Phys*. **4**, 1811 (1971).
39. M. Lipp, W.J. Evans, V. Garcia-Baonza, and H.E. Lorenzana, *J. Low Temp. Phys.* **111**, 247 (1998).
40. Don T. Cromer, David Shiferl, Richard LeSar, and Robert L. Mills, *Acta Cryst*. **C39**, 1146 (1983).